Brain Pathology ISSN 1015-6305

RESEARCH ARTICLE

# Early and Sustained Activation of Autophagy in Degenerating Axons after Spinal Cord Injury

Vinicius Toledo Ribas[1]; Bianca Schnepf[1]; Malleswari Challagundla[1]; Jan Christoph Koch[1]; Mathias Bähr[1,2]; Paul Lingor[1,2]

[1] Department of Neurology, University Medicine Göttingen; [2] Center for Nanoscale Microscopy and Molecular Physiology of the Brain (CNMPB), Göttingen, Germany.

**Keywords**
Atg5, Atg7, autophagosome, axonal lesion, LC3, ULK1.

**Corresponding author:**
Paul Lingor, MD, Department of Neurology, University Medicine Göttingen, Robert-Koch-Str. 40, Göttingen 37075, Germany (E-mail: *plingor@gwdg.de*)

Received 27 May 2014
Accepted 25 June 2014
Published Online Article Accepted 8 July 2014

The authors declare no conflict of interests.

doi:10.1111/bpa.12170

## Abstract

Axonal degeneration is one of the initial steps in many neurological disorders and has been associated with increased autophagic activity. Although there are increasing data on the regulation of autophagy proteins in the neuronal soma after spinal cord injury (SCI), their characterization in the axon is scarce. Here, we examined the regulation of autophagy during axonal degeneration in a rat model of SCI following a lesion at Th 8. We analyzed the morphological and ultrastructural changes in injured axons by immunohistochemical evaluation of autophagy-related proteins and electron microscopy at different time points following SCI. The expression of ULK1, Atg7 and Atg5 in damaged axons was rapidly upregulated within hours after SCI. The number of axonal LC3-positive autophagosomes was also rapidly increased after SCI and remained at an increased level for up to 6 weeks. Ultrastructural analysis showed early signs of axonal degeneration and increased autophagy. In conclusion, we show that autophagy is increased early and for a sustained period in degenerating axons after SCI and that it might be an important executive step involved in axonal degeneration. Therefore, autophagy may represent a promising target for future therapeutic interventions in the treatment of axonal degeneration in traumatic central nervous system disorders.

## INTRODUCTION

A number of neurological disorders have been associated with an increase in macroautophagy (here autophagy), such as neurodegenerative diseases, that is, Parkinson's disease, Alzheimer's disease, Huntington's disease or acute axonal injury (19, 28). The core molecular machinery in autophagy is comprised of proteins such as the unc-51-like kinase 1 (ULK1) that regulate the initial steps of autophagy and are localized preferentially in the autophagosome formation site, the two ubiquitin-like protein conjugation systems Atg12-Atg5-Atg16L and Atg8/LC3 that regulate later steps of autophagy as well as the E1-like enzyme Atg7 that catalyzes the conjugation reactions of Atg12 and LC3 (4, 11, 12, 24, 36). The knockdown of Atg7 and Beclin1 by RNA interference in superior cervical ganglion neurons was able to delay axonal and dendritic degeneration following growth factor withdrawal (34). It has been shown in both neurotoxin and physical injury (axotomy) models that conditional deletion of the essential autophagy mediator Atg7 in adult mice is able to preserve dopaminergic axons due to suppression of acute retrograde axonal degeneration (3). In previous studies, our group showed that local application of the autophagy inhibitor 3-methyladenine (3-MA) significantly delayed axonal degeneration and stabilized the degenerating axons following optic nerve crush lesion (19). The ultrastructural evaluation by electron microscopy (EM) showed an early appearance of LC3-positive autophagosomes, representing an early event during axonal degeneration and indicating that autophagy may represent an executive step for acute axonal degeneration (19). On the other hand, a basal level of autophagy seems to be required for the survival of neurons, as could be demonstrated by studies in knockouts for *Atg5* or *Atg7* (8, 20). This suggests that autophagy seems to be essential and continuously present in the healthy neuron, but its dysregulation during axonal injury or neurodegeneration may result in axonal degeneration and cell death.

Activation of the autophagic pathway has also been implicated in spinal cord injury (SCI). It has been shown that Beclin 1 and LC3 are upregulated in neurons, astrocytes and oligodendrocytes after SCI, and an EM analysis showed an increase of autophagosomes in the damaged neural cell bodies after SCI (2, 7, 15, 16). Although these studies focused on the neuronal cell bodies, the autophagy levels in degenerating axons after SCI have not been analyzed to date.

Axonal projections are specialized neuronal compartments and the longest parts of neurons that perform numerous functions (eg, protein synthesis and degradation) independently from the cell body (6). Degeneration of the axonal compartment is a regulated self-destructing cellular process that is mechanistically distinct from cell body death (26). Indeed, the understanding of axonal degeneration is of major importance, because in many neurological disorders, for example, amyotrophic lateral sclerosis, Parkinson's disease and traumatic SCI, the axonal degeneration precedes the loss of the cell bodies (21). Understanding the mechanisms

involved in axonal degeneration therefore is pivotal for the development of new therapeutic approaches for the treatment of SCI.

In this study, we utilized the *in vivo* rat spinal cord dorsal column lesion model to assess activation of autophagy in injured spinal cord axons. We characterize the regulation of ULK1, Atg7, Atg5 and LC3 proteins in the first hours up to 6 weeks after SCI and thus provide evidence for an early role of autophagy in axonal degeneration, pointing to autophagy as a promising target for the treatment of axonal degeneration after SCI.

## MATERIALS AND METHODS

### Animals and SCI

All animal experiments were performed with the approval of the governmental authorities and according to the legislation of the local animal research council of the State of Lower Saxony (Braunschweig), Germany. Female adult Wistar rats (250–350 g; Charles River, Sulzfeld, Germany) were used. Anesthesia was performed by i.p. injection of 2% xylazin (7 mg/kg body weight) and 10% ketamin (95 mg/kg body weight). The skin was incised and the fat layer on the back muscles was separated. After splitting of the musculature, the spinal cord was exposed via dorsal laminectomy of the thoracic level 8 (Th 8) vertebra. A dorsal hemisection (1.25 mm depth) was performed on the right side at the level of Th 8 using a pair of microscissors. This resulted in a complete axotomy of the ascending sensory and descending motor tracts (Figure 1). Control sham group rats received the same surgical procedure but no hemisection was performed. The wound was closed and animals were then left to recover under analgesia with buprenorphine (0.05 mg/kg body weight) and metamizole (1.33 mg/mL drinking water).

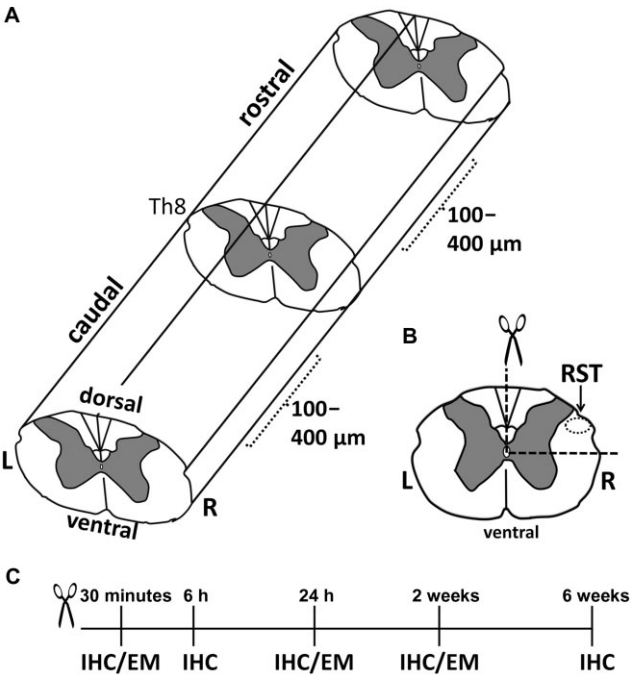


**Figure 1.** Scheme of experimental setup. A–B. The spinal cord injury (SCI) was performed at the level of Th 8 on the dorsal right side. The analysis was performed in the region of the rubrospinal tract on both sides of the lesion, rostral and caudal, over a distance of 100–400 µm. C. At the different time points after the SCI, longitudinal sections of the spinal cord tissue, including the rostral and the caudal portions of the injury site, were used for immunohistochemical (IHC) and electron microscopy (EM) analysis.

### Spinal cord tissue processing and immunostaining

For immunohistochemical evaluation, two animals each were perfused at time points 30 minutes, 6 h, 24 h, 2 weeks and 6 weeks after the dorsal hemisection procedure. For control, two animals were perfused immediately after a sham operation. The animals were perfused with 4% paraformaldehyde in phosphate-buffered saline (PBS), pH 7.4, the spinal cord was removed and postfixed in 4% paraformaldehyde in PBS overnight. Then, the spinal cord tissue was cryoprotected in an increasing series of glucose (maximum 30% glucose) and frozen at −80°C. Spinal cords were split into 1 -cm-long segments including the rostral and the caudal portion of the injury site. Longitudinal sections (16 µm thickness) through the lesion site and adjacent tissue were prepared using the cryostat (Leica, Wetzlar, Germany), collected on glass slides and used for immunohistochemical staining.

Double immunolabeling was performed with an axonal marker and different autophagy-related proteins: An antibody against phosphorylated neurofilament (SMI31, 1:500, SMI31R, Covance, Princeton, NJ, USA) was used as axonal marker. Antibodies against ULK1 (1:100, A7481, Sigma-Aldrich, St. Louis, MO, USA), Atg7 (1:100, 2631S, Cell Signaling Technology, Danvers, MA, USA), Atg5 (1:100, AP1812b, Abgent, San Diego, CA, USA) and LC3 (autophagosome marker, 1:50, sc-16756, Santa Cruz Biotechnology, Santa Cruz, CA, USA) were used to detect autophagy-related proteins. An antibody that recognizes the 150 kDa calpain-specific N-terminal α-spectrin breakdown product (27) (1:500, kind gift of R. Siman, University of Pennsylvania) was used to detect calpain-dependent cleaved α-spectrin. An antibody against oligodendrocyte myelin glycoprotein (OMgp) was used as oligodendrocyte marker (1:100, Santa Cruz Biotechnology, sc-14527). For all antibodies, antigen retrieval was carried out in citrate buffer, pH 6. Spinal cord sections were permeabilized with 0.3% Triton X-100 and 0.05% Tween 20 in PBS for 15 minutes, washed and incubated with the blocking solution (Dako Antibody Diluent, S3022, Dako, Hamburg, Germany) for at least 1 h before incubation with the primary antibodies. Then, the sections were incubated overnight at 4°C with appropriate primary antibodies diluted in the same blocking solution. To detect ULK1, Atg7, Atg5 and cleaved α-spectrin, the sections were incubated with the biotinylated secondary antibody anti-rabbit (1:200, BA-1000, Vector Laboratories, Burlinghame, CA, USA) for 1 h at 37°C, complexed with avidin- horseradish peroxidase (HRP, Vectastain ABC kit, Vector Laboratories, PK-6100) and developed with Cy3-conjugated tyramide (SAT704A001EA, Perkin Elmer, Waltham, MA, USA). To detect LC3 protein, Cy3-conjugated anti-goat IgG (1:500, 705-165-147, Jackson Immunoresearch, West Grove, PA, USA) was used for 1 h at room temperature. For axonal marker staining (phosphorylated neurofilament, SMI31), secondary antibody Cy2-conjugated anti-mouse IgG was used (Jackson

Immunoresearch, 715-226-150), and for oligodendrocyte marker (OMgp) secondary antibody Alexa Fluor 488-conjugated anti-goat was used (A-11055, Life Technologies, Carlsbad, CA, USA), both for 1 h at room temperature. The chromosomal DNA was stained with 4′,6-diamidino-2-phenylindole (DAPI, 1 μg/mL, A1001, Applichem, Darmstadt, Germany) and the sections were covered with Mowiol (Sigma, 81381). For negative controls, all procedures were identically performed, but the primary antibodies were omitted.

## Fluorescence microscopy and quantification

Microscopic optical sectioning images were taken in the region of the rubrospinal tract (RST) on both sides of the injury site, over a distance of 100–400 μm (Figure 1) using an upright fluorescence microscope (Axioplan, Zeiss, Oberkochen, Germany) equipped with an ApoTome module and AxioVision Software (Zeiss). For each group, 12 pictures in four different sections were acquired using a 40× objective lens. Axonal expression of autophagy

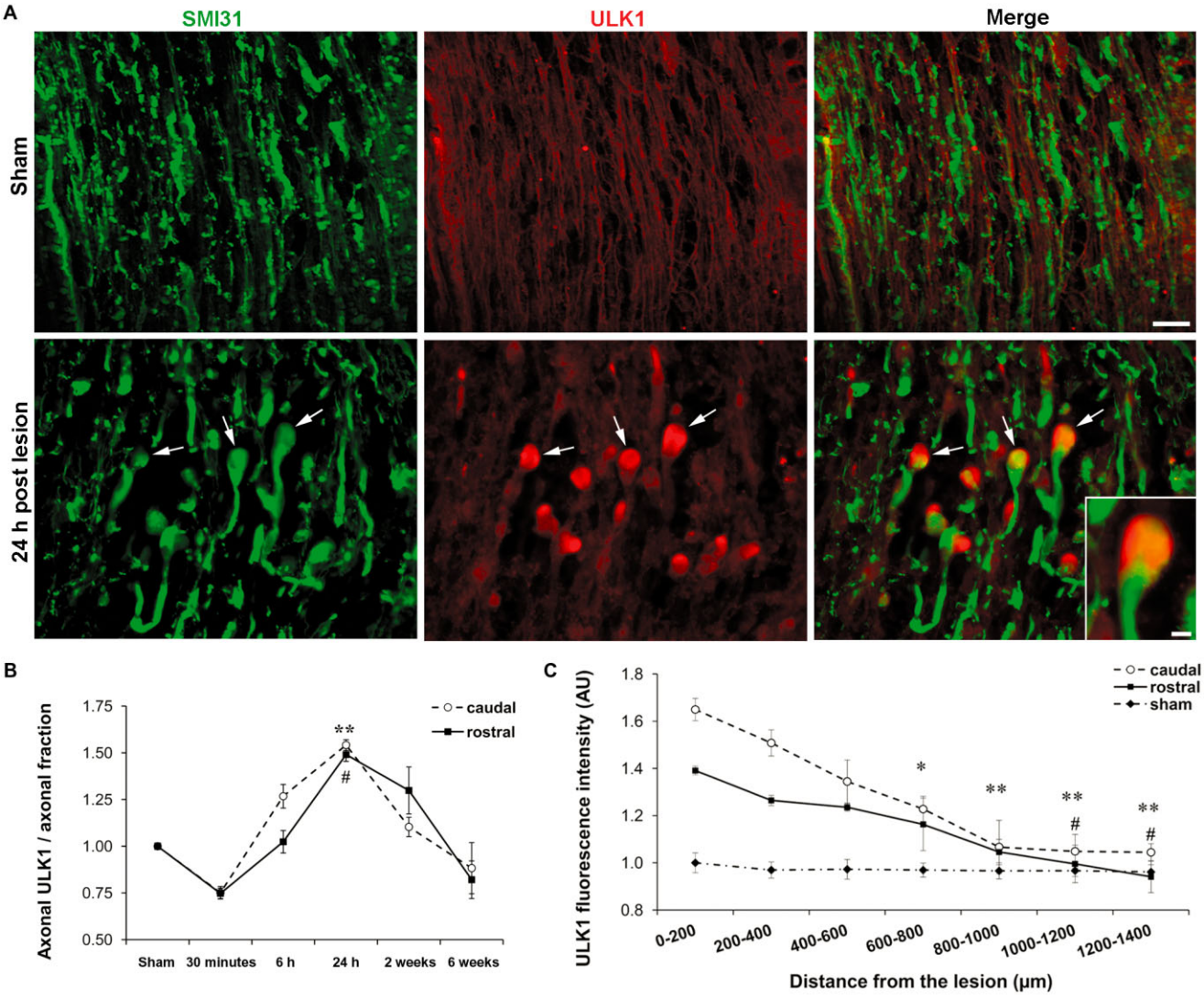


**Figure 2.** Axonal expression of ULK1 after spinal cord injury. A. Representative photomicrographs of immunohistochemistry for the axonal marker SMI31 (green) and ULK1 (red) in spinal cord longitudinal sections showing the rubrospinal tract (RST) region in the control sham operation (sham) and in the rostral side 24 h after the spinal cord injury (SCI). Arrows indicate examples of ULK1-positive axons. Scale bar: 20 μm. Inset: higher magnification showing a retraction bulb stained for ULK1. Scale bar: 5 μm. B. Quantitative analysis of ULK1 expression in axons of the RST region in the control sham operation (sham) and in the rostral and caudal sides at different time points after SCI. Data are represented as the mean of the axonal ULK1 fluorescence intensity per axonal area ± SEM. Rostral side: #$P < 0.05$ vs. sham. Caudal side: **$P < 0.01$ vs. sham. C. Quantitative analysis of total ULK1 expression in the RST region in the control sham operation (sham) and in the rostral and caudal sides in different distances from the lesion 24 h after SCI. Data are represented as the mean of the total ULK1 fluorescence intensity in every 200 μm of distance ± SEM. Rostral side: #$P < 0.05$ vs. 0–200 μm. Caudal side: *$P < 0.05$, **$P < 0.01$ vs. 0–200 μm.

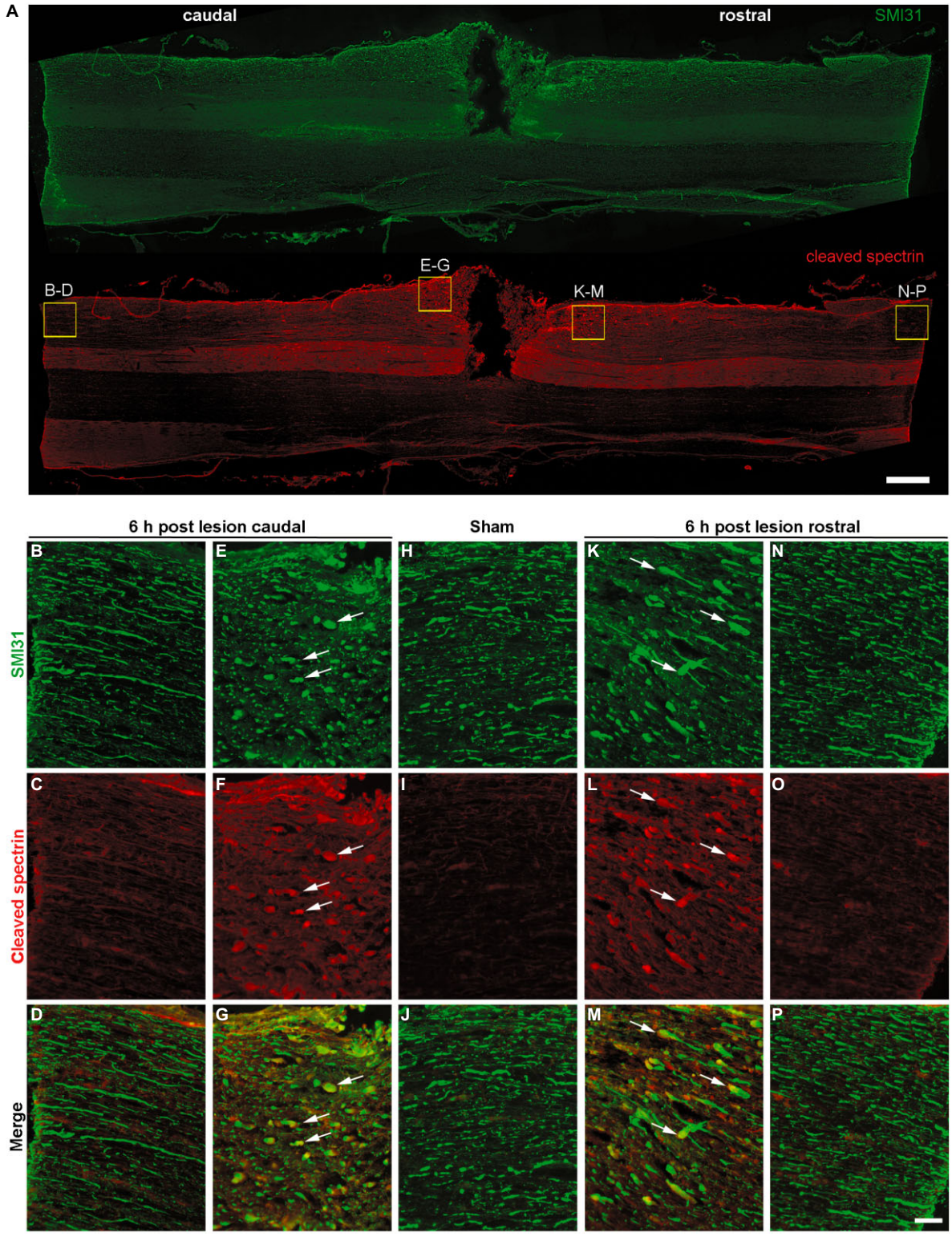


**Figure 3.** Axonal increase of cleaved spectrin after spinal cord injury (SCI). A. Overview of cleaved spectrin staining showing 1-cm spinal cord longitudinal section 6 h following SCI after immunohistochemistry for the axonal marker SMI31 (green) and cleaved spectrin (red). Scale bar: 500 μm. B–P. Representative photomicrographs showing the rubrospinal tract (RST) region in the control sham operation (sham, H–J), in the caudal (B–G) and rostral (K–P) sides 6 h after the SCI. B–G. Caudal side with a distance of approximately 5 mm (B–D) and 200 μm (E–G) from the lesion. K–P. Rostral side with a distance of approximately 200 μm (K–M) and 5 mm (N–P) from the lesion. Arrows indicate examples of cleaved spectrin-positive axons. Scale bar: 100 μm.

proteins was quantified rostral and caudal to the lesion for each different time point and the control. For quantification open access, ImageJ software (http://rsbweb.nih.gov/ij/) was used. To determine the axonal fraction per picture, the SMI31 channel pictures were first transformed to 8 bit, thresholded to a standard value for all time points and inverted. Then, the axonal fraction images were subtracted from the immunofluorescent images with labeling of autophagy proteins previously transformed to 8 bit. Finally, to determine the axonal expression of autophagy proteins, the mean pixel intensities of the resulting picture were calculated. Because of the variability of the axonal fraction over time, a ratio of the axonal autophagy protein expression and the axonal fraction was calculated and then normalized to the control. A similar quantification was performed also for LC3, where LC3-positive puncta instead of fluorescence intensity were quantified in a similar manner. For each time point, the quantification of axonal

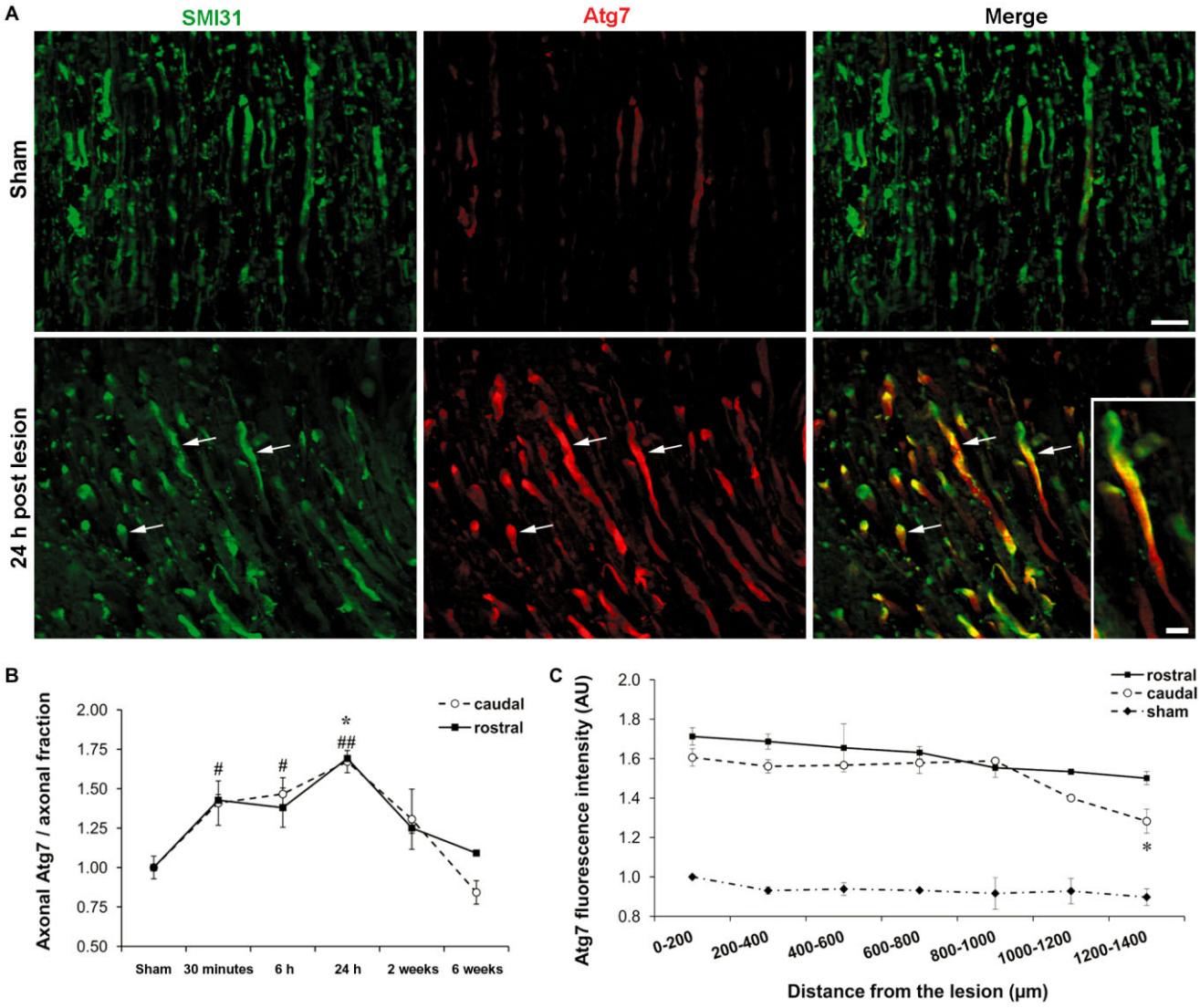


**Figure 4.** Upregulation of Atg7 in damaged axons after spinal cord injury. A. Representative photomicrographs of immunohistochemistry for the axonal marker SMI31 (green) and Atg7 (red) in spinal cord longitudinal sections showing the rubrospinal tract (RST) region in the control sham operation (sham) and in the rostral side 24 h after the spinal cord injury (SCI). Arrows indicate examples of Atg7-positive axons. Scale bar: 20 µm. Inset: higher magnification showing an axon stained for Atg7. Scale bar: 5 µm. B. Quantitative analysis of Atg7 expression in axons of the RST region in the control sham operation (sham) and in the rostral and caudal sides at different time points after SCI. Data are represented as the mean of the axonal Atg7 fluorescence intensity per axonal area ± SEM. Rostral side: #$P < 0.05$, ##$P < 0.01$ vs. sham. Caudal side: *$P < 0.05$ vs. sham. C. Quantitative analysis of total Atg7 expression in the RST region in the control sham operation (sham) and in the rostral and caudal sides in different distances from the lesion 24 h after SCI. Data are represented as the mean of the total Atg7 fluorescence intensity in every 200 µm of distance ± SEM. Caudal side: *$P < 0.05$ vs. 0–200 µm, 200–400 µm, 400–600 µm, 600–800 µm and 800–1000 µm.

autophagy protein expression per axonal fraction from the four sections was averaged per animal, and the standard error of the mean (SEM) was calculated from the mean values.

For the quantification of the total expression of autophagy proteins at different distances from the lesion site, longitudinal spinal cord sections at 24 h after the SCI were used. Images were acquired using the Axioplan microscope and MosaiX module (Zeiss). This module takes single images using a motorized stage and combines these single images to form a single overview image of the entire tissue. The whole spinal cord longitudinal section was imaged, including the region rostral and caudal to the lesion, after immunostaining with antibodies against autophagy proteins. Using ImageJ, the total fluorescence intensity of each autophagy protein staining was quantified at different distances (from 0 to 1400 μm) from the lesion and the result was plotted in a graph in intervals of 200 μm. The quantification was performed in three different sections from each animal, averaged per animal, and the SEM was calculated from the mean values.

### Electron microscopy

For EM evaluation, two animals each were perfused at time points 30 minutes, 24 h and 2 weeks after the dorsal hemisection procedure. For control, two animals were perfused immediately after a sham operation. The animals were perfused with 2% paraformaldehyde and 2% glutaraldehyde and the spinal cords were dissected and divided in 2.5-mm-long segments containing the rostral and caudal parts of the lesion site. Spinal cord segments were postfixed in 3% glutaraldehyde for 3 days and in 1% osmium tetroxide for 4 h, dehydrated in an increased series of alcohol and propylene oxide and embedded in araldite resin. Ultrathin sections (~60 nm) were prepared (Zeiss Ultracut), mounted on formvar-coated slot grids, stained with lead citrate and examined with an electron microscope (Zeiss). Pictures were taken digitally in the RST region on both sides of the injury site over a distance of approximately 100–400 μm (Figure 1). Quantifications of fiber (axoplasm and myelin sheath) diameter, axoplasm diameter and g-ratio were performed using AnalySIS software (Olympus, Tokyo, Japan).

### Statistics

For statistical analysis, a one-way analysis of variance (ANOVA) followed by Tukey's post hoc test was performed. Values were considered statistically different with a $P < 0.05$ (*), $P < 0.01$ (**) and $P < 0.001$ (***).

## RESULTS

In order to characterize the regulation of autophagy in degenerating axons after SCI, the speed of this process and its spatial distribution in relation to the lesion, we examined the expression of different autophagy proteins in the axons of the RST region on both sides of the lesion over a distance of approximately 100–400 μm (Figure 1). To establish a time course of expression of autophagy-related proteins in the axons after SCI, the animals were perfused at time points 30 minutes, 6 h, 24 h, 2 weeks and 6 weeks after the SCI.

### Upregulation of ULK1 preferentially in the retraction bulbs of degenerating axons after SCI

First, we examined the expression of ULK1, a protein involved in the initial steps of the autophagy pathway (36). Double staining with an axonal marker (SMI31) and ULK1 antibody was performed in spinal cord longitudinal sections to allow for an axon-specific evaluation of ULK1 expression. In the control sham group, the axons in the RST region were only weakly stained with the antibody against ULK1 (Figure 2A). At 30 minutes after SCI, there was an insignificant decrease of 25% in axonal ULK1 staining on both sides of the lesion. At 6 h after SCI, the axonal ULK1 expression had increased and reached a maximum at 24 h after lesion with a significant increase to 154% caudal and 149% rostral to the lesion in comparison to sham controls (Figure 2A,B). Then, the ULK1 expression started decreasing again, reaching a minimum at 6 weeks after the SCI close to the original values of the sham-operated controls (Figure 2B). The staining pattern indicated that the expression of ULK1 is mostly restricted to axons. Analyzing the ULK1 staining at a higher magnification, we

**Figure 5.** Expression of Atg5 after spinal cord injury. A. Representative photomicrographs of immunohistochemistry for the axonal marker SMI31 (green) and Atg5 (red) in spinal cord longitudinal sections showing the rubrospinal tract (RST) region in the control sham operation (sham) and in the rostral side 24 h after the spinal cord injury (SCI). Arrows indicate examples of Atg5-positive axons. Scale bar: 20 μm. Inset: higher magnification showing an axon stained for Atg5. Arrowhead points to puncta-like structures in the Atg5 staining. Scale bar: 5 μm. B. Quantitative analysis of Atg5 expression in axons of the RST region in the control sham operation (sham) and in the rostral and caudal sides at different time points after SCI. Data are represented as the mean of the axonal Atg5 fluorescence intensity per axonal area ± SEM. Rostral side: #$P < 0.05$ vs. sham. Caudal side: *$P < 0.05$ vs. sham. C. Quantitative analysis of total Atg5 expression in the RST region in the control sham operation (sham) and in the rostral and caudal sides in different distances from the lesion 24 h after SCI. Data are represented as the mean of the total Atg5 fluorescence intensity in every 200 μm of distance ± SEM. Rostral side: #$P < 0.05$ vs. 200–400 μm, 400–600 μm and 600–800 μm. Caudal side: *$P < 0.05$ vs. 0–200 μm, 200–400 μm, 400–600 μm, 600–800 μm and 800–1000 μm. D. Representative photomicrographs of immunohistochemistry for the oligodendrocyte marker oligodendrocyte myelin glycoprotein (OMgp) (green) and the autophagy protein Atg5 (red) in spinal cord longitudinal sections showing the RST region in the control sham operation (sham) and in the rostral side of the lesion 24 h after the SCI. Scale bar: 10 μm.

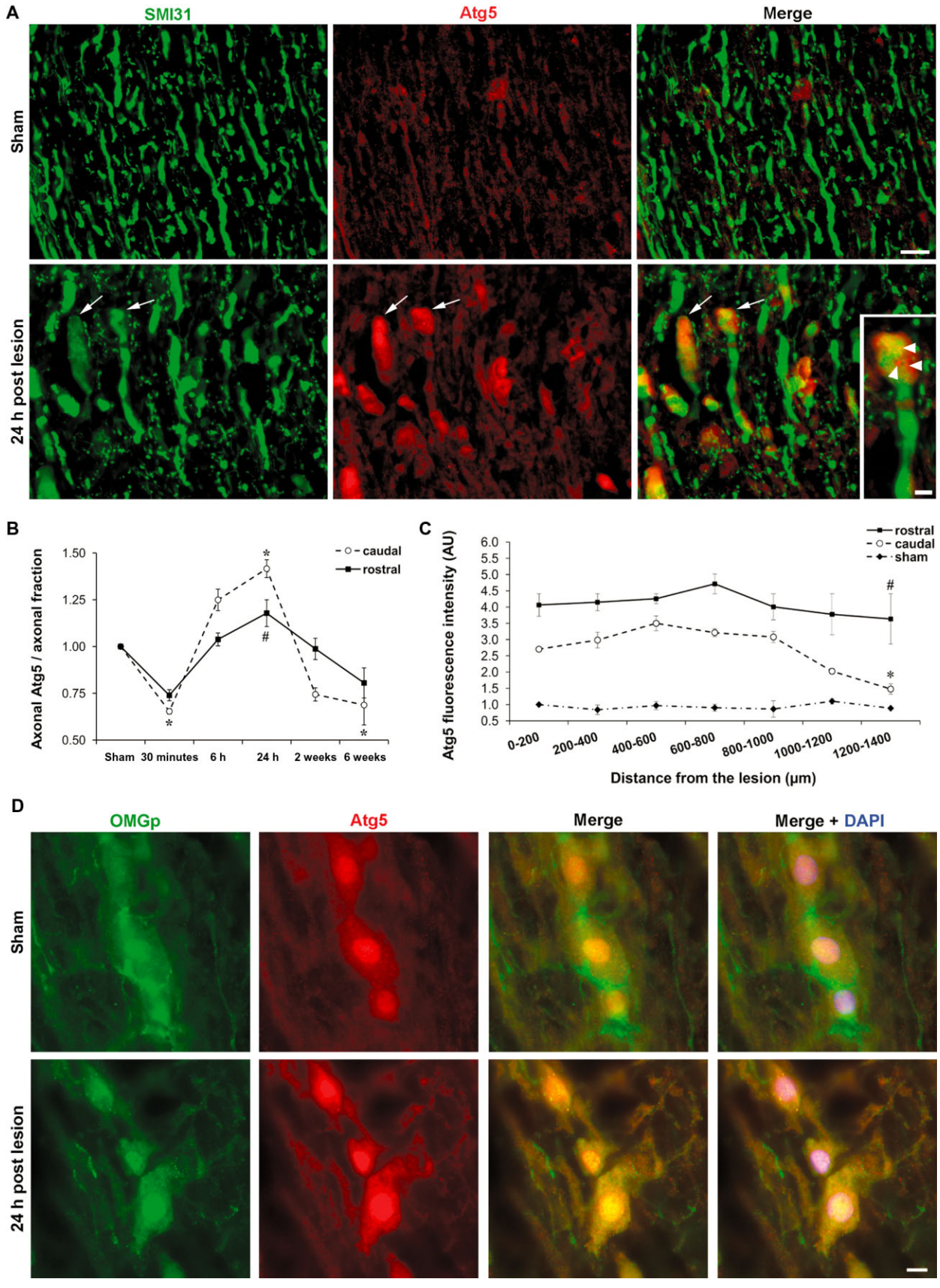

observed that the increase in ULK1 staining was most prominent in enlarged terminal regions representing retraction bulbs on both sides of the lesion (Figure 2A, inset).

To analyze if there is a variation in the ULK1 expression at different distances from the lesion, total fluorescence intensity of the ULK1 staining was measured up to 1400 μm from the lesion on both sides in longitudinal spinal cord sections at 24 h after the SCI. The total ULK1 expression was very high close to the lesion and decreased progressively at longer distances, reaching the same level as the control after 1000 μm from the lesion. Essentially, there was no difference comparing the rostral and caudal sides (Figure 2C). This result suggests that the increase in ULK1 expression after the SCI occurs mainly in regions with a short distance to the lesion on both sides.

As ULK1 stimulation was shown to be induced by calcium influx and a rapid increase in calcium in the axons and calpain-dependent spectrin cleavage was observed after SCI (5, 17, 30), we investigated if there is also an evidence for axonal calcium influx and calpain activation in our model. Double staining with SMI31 antibody and an antibody that specifically recognizes the 150-kDa fragment of calpain-mediated spectrin cleavage was performed in spinal cord longitudinal sections in the sham control group and at 6 h after SCI. In the control sham group, only a weak signal of cleaved spectrin was detected in the axons (Figure 3H–J). However, at 6 h after SCI, there was a massive increase of cleaved spectrin staining in the vicinity (approximately up to 500 μm) of the lesion (Figure 3A,E–G,K–M). At longer distances from the lesion, the cleaved spectrin staining decreased markedly on both sides of the lesion (Figure 3A,B–D,N–P). These results corroborate prominent influx of calcium after lesion and subsequent activation of calpain in damaged axons close to the lesion after SCI.

## Damaged axons show increased Atg7 expression after SCI

To evaluate the time course of Atg7 expression in the axons after SCI, double immunostainings for SMI31 and Atg7 were performed in spinal cord longitudinal sections at different time points after SCI, similar to the evaluation of ULK1 expression. Only weak or no immunofluorescence for Atg7 was found in the control sham group (Figure 4A). Already at 30 minutes after the SCI, an increase by approximately 40% in axonal Atg7 staining on both sides of the lesion could be observed. At 6 h after the SCI the Atg7 expression was similar to 30 minutes, and at 24 h a maximum axonal Atg7 expression was reached with an increase by approximately 70% on both sides of the lesion (Figure 4A,B). Then, the axonal Atg7 expression dropped at 2 weeks, reaching a minimum at 6 weeks after the SCI close to the initial values of the sham-operated control (Figure 4B). In contrast to the expression of ULK1, the Atg7 staining was rather diffuse in the entire axon (Figure 4A, inset). Similar to ULK1, the Atg7 staining was restricted to the axons (Figure 4A).

The evaluation of the total Atg7 expression at different distances from the lesion showed only a very slight decrease in Atg7 expression at longer distances from the lesion compared with distances close to the lesion, which only became significant at 1200–1400 μm caudal to the lesion (Figure 4C). This is in contrast to the clear decrease of ULK1 fluorescence as a function of distance from the lesion site.

## Atg5 is upregulated after SCI

After analysis of ULK1 and Atg7, we characterized the regulation of Atg5, which is essential for autophagosome formation and localizes to the crescent-shaped autophagosome precursors (4). In parallel to ULK1 and Atg7, there was only a weak Atg5 staining observed in the axons of the RST region in the control sham group (Figure 5A). The time course of axonal Atg5 expression showed a slight decrease by ~25% at 30 minutes after the SCI. At 6 h after the SCI there was an increase in Atg5 staining, and at 24 h after the SCI a maximum axonal expression of Atg5 was reached, which was stronger caudal to the lesion than rostral to it. Then, the axonal Atg5 expression dropped at 2 weeks, reaching a minimum at 6 weeks after the SCI (Figure 5B). These results suggest that the axonal expression of Atg5 could be regulated in a similar manner as ULK1 expression with regard to its time course. Total expression of Atg5 remained at rather high levels within the 1400 μm rostral and caudal to the lesion, except for the most distal caudal regions, where expression significantly decreased almost reaching control values (Figure 5C). Similar to ULK1, higher magnification images revealed that the majority, but not all, of the axonal Atg5 staining was localized to the retraction bulbs on both sides of the lesion (Figure 5A, inset). In addition, we observed the formation of some Atg5-positive puncta-like structures in the retraction bulbs (Figure 5A, inset—arrowhead). We could also show that Atg5 expression was not only restricted to axons, but was also found in oligodendrocytes in sham-operated and lesioned animals, in contrast to expression of ULK1 and Atg7 that were restricted to axons (Figure 5D).

## Early and sustained increase in LC3-positive puncta after SCI

Finally, we examined the expression of LC3 in SMI31-positive axons following SCI. In the control sham group, the number of axonal LC3-positive puncta was very low (Figure 6A). Their numbers started to increase as early as 30 minutes after lesion. At 6 h, their number was increased by ~60% and reached significantly higher values (166% rostral and 178% caudal to the lesion of sham-lesioned controls) at 2 weeks after lesion. Thereafter, numbers of axonal LC3 puncta started to decline slightly, but remained still at a high level even 6 weeks after SCI (157% of the sham-lesioned controls) (Figure 6B). The LC3-positive puncta were localized in the entire axon, similar to the Atg7 staining (Figure 6A). No significant differences were observed between numbers of LC3-positive autophagosomes rostral vs. caudal to the lesion site. We also observed that the LC3-positive puncta were not exclusive to axons (Figure 6A).

## Ultrastructural alterations of degenerating axons after SCI

After immunohistochemical characterization, we used EM to qualitatively and quantitatively examine the ultrastructure of axons in the RST after SCI. The animals were perfused after control sham operation and at time points 30 minutes, 24 h and 2 weeks

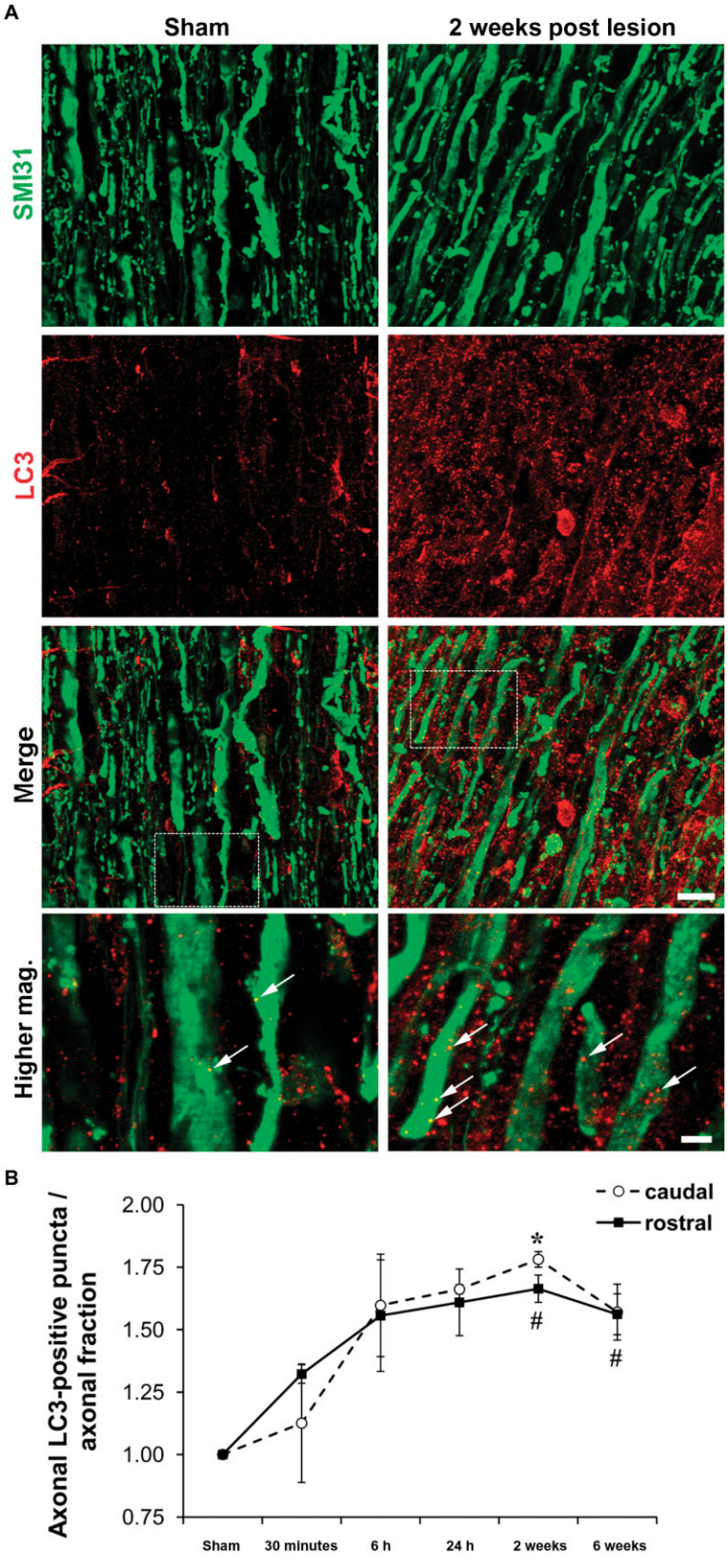


**Figure 6.** Immunohistochemical analysis of LC3-positive autophagosomes in damaged axons after spinal cord injury. A. Representative photomicrographs of immunohistochemistry for the axonal marker SMI31 (green) and LC3 (red) in spinal cord longitudinal sections showing the rubrospinal tract (RST) region in the control sham operation (sham) and in the rostral side 2 weeks after the spinal cord injury (SCI). Scale bar: 20 μm. Inset: higher magnification showing axons stained for LC3-positive autophagosomes. Arrows indicate examples of axonal LC3-positive autophagosomes. Scale bar: 5 μm. B. Quantitative analysis of LC3-positive autophagosome number in axons of the RST region in the control sham operation (sham) and in the rostral and caudal sides at different time points after SCI. Data are represented as the mean of the axonal LC3-positive autophagosome number per axonal area ± SEM. Rostral side: #$P < 0.05$ vs. sham. Caudal side: *$P < 0.05$ vs. sham.

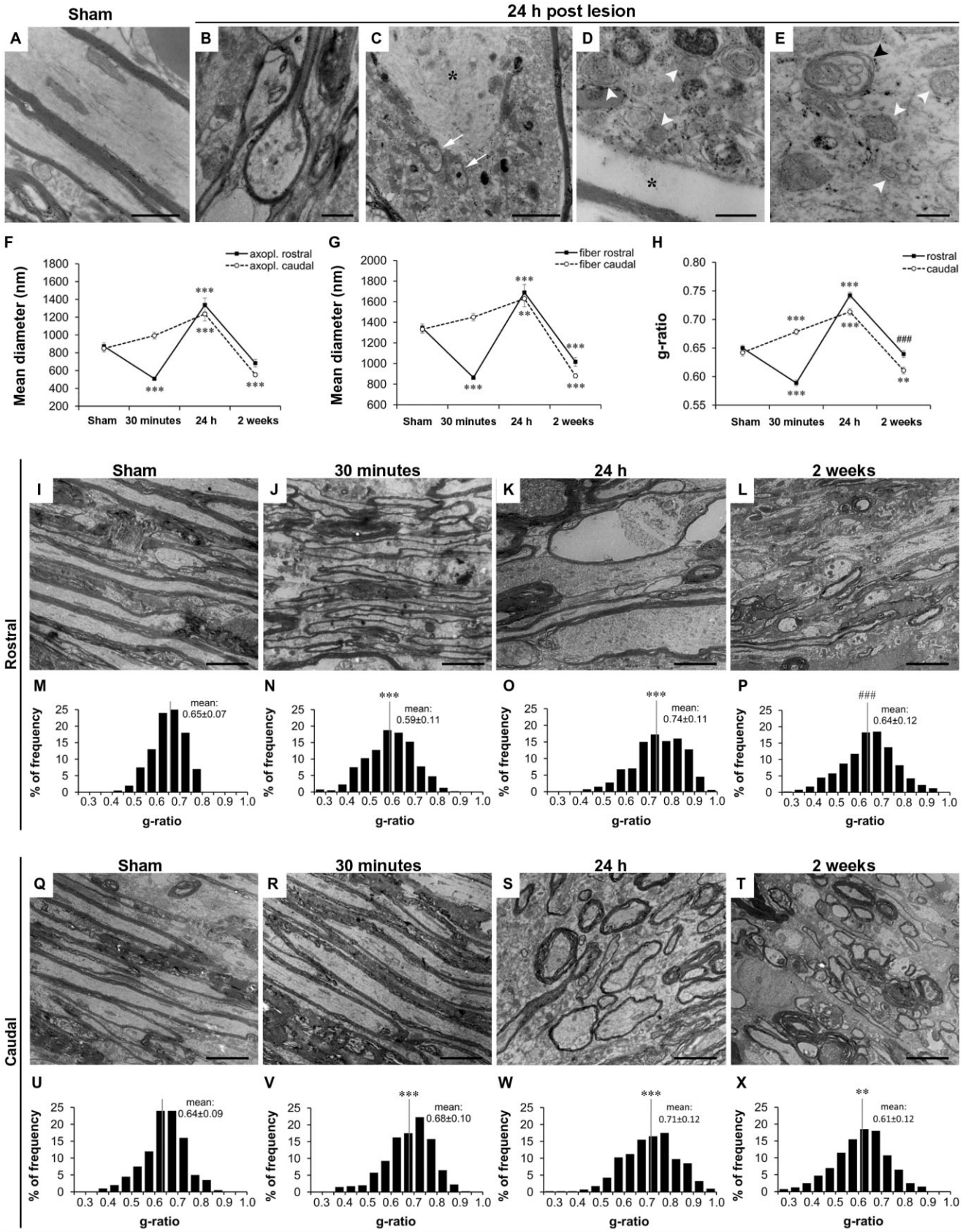

after the dorsal hemisection procedure. The EM showed that 24 h after the SCI, there was an enrichment of axonal bulbs in the damaged tissue (Figure 7B). These axonal bulbs showed structural alterations such as axonal swellings with densely packed organelles, mostly damaged mitochondria and vacuoles, and disintegrated cytoskeleton (Figure 7C). Mitochondria displayed structural signs of degradation, that is, swelling and cisternal dilatation (Figure 7C). In a higher magnification, we observed that these axonal fragments have a strong vacuolization of the axoplasm, and the axoplasm was detached from the myelin sheath (Figure 7D). Accumulation of cell organelles can be identified as mitochondria and bilayered vacuoles in the sense of autophagic vacuoles (Figure 7C–E). In contrast, the axons in the control sham-operated group showed a regular parallel orientation without swellings or bulbs. Mitochondria were not swollen or fragmented and the cytoskeleton appeared consistent and did not display any structural signs of dysfunction (Figure 7A,I,Q). These results suggest that SCI induces rapid morphological changes in the close vicinity to the lesion and that this is accompanied by a rapid increase of autophagosomes in the damaged axons.

The quantitative analysis showed that the mean fiber diameter rapidly decreased significantly from $1345 \pm 38$ nm in control sham-operated animals to $863 \pm 20$ nm rostral to the lesion already at 30 minutes after SCI. Caudal to the lesion, the mean fiber diameter increased slightly from $1332 \pm 39$ nm in controls to $1450 \pm 37$ nm at 30 minutes after SCI. At 24 h after the SCI, the mean fiber diameter reached the maximum value of $1689 \pm 77$ nm at the rostral side and of $1630 \pm 78$ nm at the caudal side (Figure 7G). At this time point, many enlarged axons reaching diameters higher than 5000 nm can be found on both sides of the lesion. At 2 weeks after the SCI, the mean fiber diameter decreased to $1081 \pm 65$ nm at the rostral side and $958 \pm 44$ nm at the distal side, which was lower than fiber diameters in the sham-operated control animals (Figure 7G).

The mean g-ratio (axoplasm diameter divided by fiber diameter) changed rapidly after SCI, decreasing on the rostral side from $0.65 \pm 0.07$ in the control sham group to $0.59 \pm 0.11$ at 30 minutes after SCI, and increasing on the caudal side from $0.64 \pm 0.09$ in the control sham group to $0.68 \pm 0.10$ at 30 minutes after SCI. At 24 h after SCI the maximum mean value of g-ratio was reached (rostral side: $0.74 \pm 0.11$ and caudal side: $0.71 \pm 0.12$), and at 2 weeks after the SCI the mean g-ratio decreased again to $0.64 \pm 0.12$ at the rostral side and $0.61 \pm 0.12$ at the caudal side to the lesion (Figure 7H). An increasing degree of dispersion of the g-ratio was found after the SCI on both sides of the lesion as witnessed by the increased standard deviation at the later time points (Figure 7M–P,U–X). These data represent the increasing heterogeneity of axonal morphologies following SCI with some axons having a thin diameter while others displaying a massively increased diameter, especially at the time points of 24 h and 2 weeks after the SCI (Figure 7K,L,O,P,S,T,W,X).

## DISCUSSION

The present study addressed the extent of autophagy in axons of the lesioned RST by quantification of several proteins with high relevance for the autophagy cascade. While the basal expression of ULK1, Atg7, Atg5 and LC3 in the axons of the sham-operated control group was very low, there was a rapid increase in the overall axonal expression of these proteins following axonal lesion. Their maximum intra-axonal expression peaked within 24 h after lesion, with the exception of LC3, which showed the most prominent expression at 2 weeks after SCI. Interestingly, the increase in ULK1 expression was most prominent in close vicinity to the lesion site, while Atg7 and Atg5 showed a more widespread increase in expression. The ultrastructural analysis revealed signs of axonal degeneration and increased autophagy such as axonal swellings and accumulation of autophagosomes surprisingly early and persisting several weeks after SCI (Figure 8).

The ULK1 protein is the predominant isoform, among the other ULK proteins, involved in autophagy (1). It is a critical autophagy-related protein localized at the top of the autophagic pathway that receives signals from the nutrient sensors mTOR (mammalian target of rapamycin) and AMPK (AMP-activated protein kinase) (9, 13, 29). Interestingly, the preferentially subcellular localization of ULK1 on the retraction bulbs of damaged axons and the increased ULK1 expression in the close vicinity of both sides of the lesion suggest that ULK1 may be an early initiating protein of the autophagy cascade in the spinal cord, and that this activation may be triggered initially in the retraction bulbs. Our group showed previously that the accumulation of autophagosomes in optic nerve axons after crush lesion is dependent on calcium influx, and interestingly an increase in axonal calcium influx was also reported after SCI (19, 30). The increase in calpain cleavage of spectrin in damaged axons in our model indicates an increase of calcium influx, as calpain is activated by calcium. In addition,

**Figure 7.** Ultrastructural analysis of degenerating axons after spinal cord injury. Representative electron microscopy images of longitudinal sections showing axons in the rubrospinal tract (RST) region in the control sham operation (A) and in the rostral side 24 h after the spinal cord injury (SCI) (B–E). B. At 24 h after the SCI, axon fragments form bulb-like structures. C. A swollen axon with accumulation of organelles, mostly mitochondria (arrows point to swollen mitochondria) located in a disintegrated cytoskeleton (asterisk). D. Accumulation of autophagic vacuoles (white arrowhead) and detachment of the axoplasm from the myelin sheath (asterisk). E. Some autophagic vacuoles enriched with cellular material (white arrowhead) and organelles (black arrowhead). Scale bars: 1 μm (A–C) and 200 nm (D and E). Quantification of the mean axoplasm (F) and fiber (G) diameter over time. Data are represented as the mean ± SEM. $^{**}P < 0.01$, $^{***}P < 0.001$ vs. sham. H. Quantification of the mean g-ratio (axoplasm diameter divided by fiber diameter) over time. Data are represented as the mean ± SEM. $^{**}P < 0.01$, $^{***}P < 0.001$ vs. sham; $^{\#\#\#}P < 0.001$ vs. rostral 24 h and 30 minutes. Sham, N = 200; 30 minutes, 24 h and 2 weeks, N = 400. Overview of the spinal cord RST axons in the control sham operation (I and Q), rostral side 30 minutes (J), 24 h (K) and 2 weeks (L) after SCI, and caudal side 30 minutes (R), 24 h (S) and 2 weeks (T) after SCI. Scale bars: 3 μm. Histograms of g-ratios of spinal cord RST axons (M–P and U–X) (in % frequency, bin width 0.05). Data are represented as the mean ± SD. $^{**}P < 0.01$, $^{***}P < 0.001$ vs. sham; $^{\#\#\#}P < 0.001$ vs. rostral 24 h and 30 minutes. Sham, N = 200; 30 minutes, 24 h and 2 weeks, N = 400.

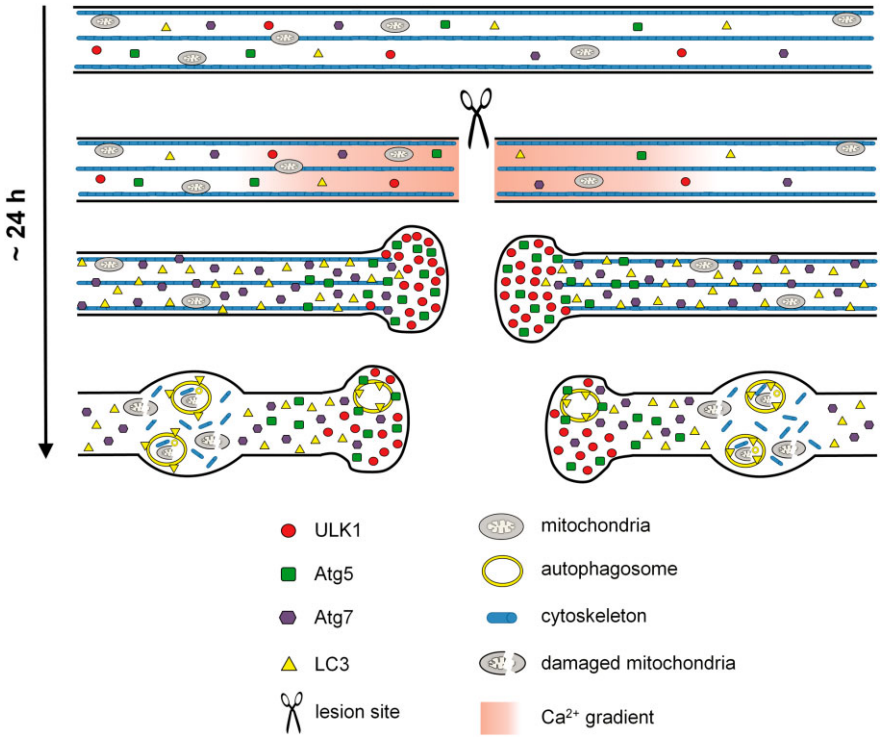


**Figure 8.** Scheme of the morphological events observed in damaged axons after spinal cord injury (SCI). Before lesion, the basal axonal levels of the autophagy-related proteins ULK1, Atg7, Atg5 and LC3 are very low. Injury to the axons of the spinal cord induces a rapid influx of calcium that could activate the autophagy cascade through ULK1 stimulation, which strongly accumulates in the retraction bulbs. The Atg7 protein, which activates Atg5 and LC3 and is localized downstream from ULK1 in the autophagy pathway, shows an increased expression throughout the damaged axons and could contribute to the spatial propagation of the autophagy cascade. Atg5 also accumulates in the retraction bulbs and might foster autophagosome biogenesis in cooperation with LC3. Finally, a misalignment of the cytoskeletal network and an accumulation of damaged organelles in axonal swellings can be seen 24 h after SCI. This occurs concomitantly with the appearance of a high number of autophagic vacuoles enriched with cellular material and organelles in axonal swellings on both sides, rostral and caudal, to the lesion site.

calcium influx induced by amino acid starvation regulates autophagy through activation of $Ca^{2+}$/calmodulin-dependent kinase kinase-β/AMPK pathways and inhibition of mTOR, which results in ULK1 stimulation (5). Thus, one hypothesis for the accumulation of ULK1 and consequent autophagy activation in retraction bulbs is calcium influx to this region due to membrane disruption and via calcium channels after SCI similar to what has previously been shown in optic nerve crush injury (19). Furthermore, the major increase in ULK1 expression occurs up to 400 µm from the lesion center, which corresponds to the area where calpain is activated and that will degenerate due to acute axonal degeneration (17), suggesting that ULK1 might be an active player in this process.

We also show that Atg7 is significantly upregulated in damaged axons after SCI, but this upregulation is nearly constant within the first 1200 µm rostral and caudal to the lesion. Atg7 is essential for autophagosome biogenesis, as it acts like an E1 enzyme to mediate the conjugation reactions of the two ubiquitin-like proteins Atg12-Atg5 and Atg8/LC3 (4, 11, 24). Although the autophagy cascade may be activated in the retraction bulbs, our data suggest that the autophagic cascade might be rapidly propagated to more distal axonal compartments and that Atg7 may play a major role in this long-distance propagation along the axon. Homeostasis of Atg7 seems finely tuned, as its specific ablation in unlesioned Purkinje cells cause a progressive axonal dystrophy (20).

The Atg5 protein is part of a large complex, which includes Atg12 and Atg16L. It is localized in the membrane of the autophagosome precursor (phagophore) and dissociates from it after autophagosome completion, playing an essential role in autophagosome development (23, 25). Our study shows an upregulation of Atg5 in damaged axons after SCI and its major increase occurs in retraction bulbs on both sides of the lesion similar to ULK1. In addition, we identified in the retraction bulbs the formation of some puncta-like structures showing Atg5 expression. Previous studies showed that the autophagosome biogenesis occurs in the distal ends of unlesioned and lesioned neurites (22, 35, 37). As ULK1, which is involved in autophagy induction and localizes in the autophagosome formation site (12), and Atg5, which is involved in autophagosome biogenesis and is attached to the membrane of the phagophore (25), are both localized in the retraction bulbs, we can speculate that in spinal cord the retraction bulbs on both sides of the lesion could be the site where autophagosome production is initiated after axonal damage. Widespread increase in Atg5 expression could be related to the similar distribution of Atg7, which facilitates conjugation of Atg5 and Atg12 (4). In addition, the Atg5 expression was not restricted to axons. We also found high levels of Atg5 expression, but not the other autophagy proteins, in oligodendrocytes in the sham control group as well as in lesioned animals. Previous studies showed the expression of other autophagy proteins, for example, LC3 and Beclin1, in oligodendrocytes after SCI (15, 16). However, the role of autophagy in oligodendrocytes after axonal injury is still unclear.

The LC3 protein regulates autophagosome formation and expansion, and its active form (LC3-II) becomes inserted into the membrane of the autophagosome and is used extensively as an autophagosome marker (14, 18). We demonstrated a robust and sustained increase in axonal LC3-positive autophagosome numbers after SCI. Interestingly, the LC3-positive puncta were not exclusive to axons. An increase in the expression of LC3 in oligodendrocytes after SCI was already shown previously (16), suggesting that the LC3-positive puncta outside of the axons might

be localized in the myelin sheath. The maximum increase in the axonal levels of LC3 occurred only at 2 weeks after the lesion, which was long after the maximum increase observed for ULK1, Atg7 and Atg5. As LC3 is inserted in the autophagosome membrane until its fusion with lysosomes, and the autophagosomes is transported through neuritis (14, 22, 35, 37), it is reasonable that the increase of LC3 is not restricted to a specific axonal compartment. Compartment-unspecific studies showed that the number of LC3-positive cells rapidly increases in the lesion site after SCI and starts to decrease after 3 days (10, 16, 32). In contrast, we show here that the number of axonal LC3-positive autophagosomes remains at an increased level for at least 2 weeks after SCI, and only then starts to decrease slightly. Moreover, the number of axonal LC3-positive autophagosomes remained at an increased level for up to 6 weeks after lesion. LC3 expression thus follows the widespread expression of Atg7 and Atg5 with a temporal delay. We thus hypothesize that sustained activation of autophagy contributes to chronic effects, such as late axonal degeneration, in models of SCI.

The ultrastructural analysis showed early signs of axonal degeneration such as axonal swellings starting at 30 minutes and more prominently at 24 h after SCI, which is the time point where we found the maximal expression of the autophagy proteins ULK1, Atg7 and Atg5. Previous studies showed this early appearance of ultrastructural alterations in damaged axons within hours after optic nerve crush and at 48 h after spinal cord lesion (19, 31). In addition to the axonal degeneration, we observed an accumulation of autophagosomes in damaged axons after SCI, corroborating the quantification of axonal LC3-positive autophagosomes. The accumulation of autophagosomes on damaged axons has been shown in other models of neurite degeneration and could be due to an increase in autophagosome production exceeding the rate of their clearance, leading to an accumulation of autophagosomes in axonal swellings (33).

Interestingly, we did not find marked differences between the rostral and caudal sides of the lesion in regard to autophagy protein expression and ultrastructural alterations with the exception of axonal diameter and g-ratio at 30 minutes after SCI. However, at all the later time points, the ultrastructural alterations were similar rostral and caudal to the lesion. Previous *in vivo* live imaging studies showed that axonal ends to both sides of the lesion die back symmetrically in the first 30 h after SCI, having some similarities such as the formation of bulb-like structures in axonal tips and the activation of calpain (17). It is only after ~30 h when the rostral and caudal axonal degeneration pathways start to diverge when rostral axons show a slow axonal retraction, and caudal axons suddenly begin to rapidly fragment due to Wallerian degeneration (17). In our study, we showed the most prominent alterations in autophagy levels and axonal degeneration up to 24 h on both sides of the lesion, and we did not analyze time points between 24 h and 2 weeks. This suggests that early axonal degeneration both rostral and caudal to the lesion may be activated by common mechanisms of axonal self-destruction, which in addition to calpain activation could be the autophagy pathway.

Taken together, we describe here an early and sustained increase of key players of the autophagic cascade in the lesioned axonal compartment, suggesting that autophagy might be an important initiating and executive step involved in axonal degeneration following traumatic injury. This early upregulation of autophagy-related proteins points to them as promising therapeutic targets for the modulation of autophagy and axonal degeneration following traumatic spinal cord lesions.

## ACKNOWLEDGMENTS

We thank Lisa Barski and Vivian Dambeck for excellent technical assistance. We thank Robert Siman from University of Pennsylvania for the kind gift of the calpain-specific cleaved α-spectrin antibody. We thank Brigitte Maruschak, Christine Stadelmann-Nessler and Wolfgang Brück for providing the EM facilities and helping with the ultrastructural analysis. Paul Lingor was funded by the International Foundation for Research in Paraplegia (IRP-P 112) and the Deutsche Forschungsgemeinschaft (DFG-LI 1308/3-1). Vinicius Toledo Ribas is a fellow of the National Council for Scientific and Technological Development (CNPq), Brazil.

## REFERENCES

1. Chan EYW, Kir S, Tooze SA (2007) Sirna screening of the kinome identifies ULK1 as a multidomain modulator of autophagy. *J Biol Chem* **282**:25464–25474.
2. Chen H-C, Fong T-H, Lee A-W, Chiu W-T (2012) Autophagy is activated in injured neurons and inhibited by methylprednisolone after experimental spinal cord injury. *Spine (Phila. PA. 1976)* **37**:470–475.
3. Cheng H-C, Kim SR, Oo TF, Kareva T, Yarygina O, Rzhetskaya M *et al* (2011) Akt suppresses retrograde degeneration of dopaminergic axons by inhibition of macroautophagy. *J Neurosci* **31**:2125–2135.
4. Geng J, Klionsky DJ (2008) The atg8 and atg12 ubiquitin-like conjugation systems in macroautophagy. "Protein modifications: beyond the usual suspects" review series. *EMBO Rep* **9**:859–864.
5. Ghislat G, Patron M, Rizzuto R, Knecht E (2012) Withdrawal of essential amino acids increases autophagy by a pathway involving Ca2+/calmodulin− dependent kinase kinase- (CaMKK-). *J Biol Chem* **287**:38625–38636.
6. Gumy LF, Tan CL, Fawcett JW (2010) The role of local protein synthesis and degradation in axon regeneration. *Exp Neurol* **223**:28–37.
7. Hao H-H, Wang L, Guo Z-J, Bai L, Zhang R-P, Shuang W-B *et al* (2013) Valproic acid reduces autophagy and promotes functional recovery after spinal cord injury in rats. *Neurosci Bull* **29**:484–492.
8. Hara T, Nakamura K, Matsui M, Yamamoto A, Nakahara Y, Suzuki-Migishima R *et al* (2006) Suppression of basal autophagy in neural cells causes neurodegenerative disease in mice. *Nature* **441**:885–889.
9. Hosokawa N, Hara T, Kaizuka T, Kishi C, Takamura A, Miura Y *et al* (2009) Nutrient-dependent mtorc1 association with the ULK1-Atg13-FIP200 complex required for autophagy. *Mol Biol Cell* **20**:1981–1991.
10. Hou H, Zhang L, Zhang L, Tang P (2014) Acute spinal cord injury in rats should target activated autophagy. *J Neurosurg Spine* **20**:568–577.
11. Ichimura Y, Kirisako T, Takao T, Satomi Y, Shimonishi Y, Ishihara N *et al* (2000) A ubiquitin-like system mediates protein lipidation. *Nature* **408**:488–492.
12. Itakura E, Mizushima N (2010) Characterization of autophagosome formation site by a hierarchical analysis of mammalian atg proteins. *Autophagy* **6**:764–776.

13. Jung CH, Jun CB, Ro S-H, Kim Y-M, Otto NM, Cao J *et al* (2009) ULK-Atg13-FIP200 complexes mediate mTOR signaling to the autophagy machinery. *Mol Biol Cell* **20**:1992–2003.
14. Kabeya Y, Mizushima N, Ueno T, Yamamoto A, Kirisako T, Noda T *et al* (2000) LC3, a mammalian homologue of yeast Apg8p, is localized in autophagosome membranes after processing. *EMBO J* **19**:5720–5728.
15. Kanno H, Ozawa H, Sekiguchi A, Itoi E (2009) Spinal cord injury induces upregulation of Beclin 1 and promotes autophagic cell death. *Neurobiol Dis* **33**:143–148.
16. Kanno H, Ozawa H, Sekiguchi A, Yamaya S, Itoi E (2011) Induction of autophagy and autophagic cell death in damaged neural tissue after acute spinal cord injury in mice. *Spine (Phila, PA 1976)* **36**:E1427–E1434.
17. Kerschensteiner M, Schwab ME, Lichtman JW, Misgeld T (2005) *In vivo* imaging of axonal degeneration and regeneration in the injured spinal cord. *Nat Med* **11**:572–577.
18. Klionsky DJ, Abdalla FC, Abeliovich H, Abraham RT, Acevedo-Arozena A, Adeli K *et al* (2012) Guidelines for the use and interpretation of assays for monitoring autophagy. *Autophagy* **8**:445–544.
19. Knöferle J, Koch JC, Ostendorf T, Michel U, Planchamp V, Vutova P *et al* (2010) Mechanisms of acute axonal degeneration in the optic nerve *in vivo*. *Proc Natl Acad Sci USA* **107**:6064–6069.
20. Komatsu M, Wang QJ, Holstein GR, Friedrich VL, Iwata J, Kominami E *et al* (2007) Essential role for autophagy protein atg7 in the maintenance of axonal homeostasis and the prevention of axonal degeneration. *Proc Natl Acad Sci USA* **104**:14489–14494.
21. Lingor P, Koch JC, Tönges L, Bähr M (2012) Axonal degeneration as a therapeutic target in the CNS. *Cell Tissue Res* **349**:289–311.
22. Maday S, Wallace KE, Holzbaur ELF (2012) Autophagosomes initiate distally and mature during transport toward the cell soma in primary neurons. *J Cell Biol* **196**:407–417.
23. Mizushima N, Kuma A, Kobayashi Y, Yamamoto A, Matsubae M, Takao T *et al* (2003) Mouse apg16l, a novel wd-repeat protein, targets to the autophagic isolation membrane with the apg12-apg5 conjugate. *J Cell Sci* **116**:1679–1688.
24. Mizushima N, Noda T, Yoshimori T, Tanaka Y, Ishii T, George MD *et al* (1998) A protein conjugation system essential for autophagy. *Nature* **395**:395–398.
25. Mizushima N, Yamamoto A, Hatano M, Kobayashi Y, Kabeya Y, Suzuki K *et al* (2001) Dissection of autophagosome formation using apg5-deficient mouse embryonic stem cells. *J Cell Biol* **152**:657–668.
26. Raff MC, Whitmore A V, Finn JT (2002) Axonal self-destruction and neurodegeneration. *Science* **296**:868–871.
27. Roberts-Lewis JM, Savage MJ, Marcy VR, Pinsker LR, Siman R (1994) Immunolocalization of calpain i-mediated spectrin degradation to vulnerable neurons in the ischemic gerbil brain. *J Neurosci* **14**:3934–3944.
28. Rubinsztein DC, Difiglia M, Heintz N, Nixon RA, Qin Z, Ravikumar B *et al* (2005) Autophagy and its possible roles in nervous system diseases. *Autophagy* **1**:11–22.
29. Shang L, Chen S, Du F, Li S, Zhao L, Wang X (2011) Nutrient starvation elicits an acute autophagic response mediated by ULK1 dephosphorylation and its subsequent dissociation from AMPK. *Proc Natl Acad Sci USA* **108**:4788–4793.
30. Shi Y, Kim S, Huff TB, Borgens RB, Park K, Shi R, Cheng J-X (2010) Effective repair of traumatically injured spinal cord by nanoscale block copolymer micelles. *Nat Nanotechnol* **5**:80–87.
31. Smith PM, Jeffery ND (2006) Histological and ultrastructural analysis of white matter damage after naturally-occurring spinal cord injury. *Brain Pathol* **16**:99–109.
32. Tang P, Hou H, Zhang L, Lan X, Mao Z, Liu D *et al* (2013) Autophagy reduces neuronal damage and promotes locomotor recovery via inhibition of apoptosis after spinal cord injury in rats. *Mol Neurobiol* **49**:276–287.
33. Yang Y, Coleman M, Zhang L, Zheng X, Yue Z (2013) Autophagy in axonal and dendritic degeneration. *Trends Neurosci* **36**:418–428.
34. Yang Y, Fukui K, Koike T, Zheng X (2007) Induction of autophagy in neurite degeneration of mouse superior cervical ganglion neurons. *Eur J Neurosci* **26**:2979–2988.
35. Yang Y, Xu K, Koike T, Zheng X (2008) Transport of autophagosomes in neurites of pc12 cells during serum deprivation. *Autophagy* **4**:243–245.
36. Yang Z, Klionsky DJ (2010) Mammalian autophagy: core molecular machinery and signaling regulation. *Curr Opin Cell Biol* **22**:124–131.
37. Yue Z (2007) Regulation of neuronal autophagy in axon: implication of autophagy in axonal function and dysfunction/degeneration. *Autophagy* **3**:139–141.